Journal of Solid Mechanics Vol. 8, No. 3 (2016) pp. 645-661

Nonlocal Bending Analysis of Bilayer Annular/Circular Nano Plates Based on First Order Shear Deformation Theory

Sh. Dastjerdi , M. Jabbarzadeh *

Department of Mechanical Engineering, Mashhad Branch, Islamic Azad University, Mashhad, Iran

Received 25 June 2016; accepted 27 August 2016

ABSTRACT

In this paper, nonlinear bending analysis of bilayer orthotropic annular/circular graphene sheets is studied based on the nonlocal elasticity theory. The equilibrium equations are derived in terms of generalized displacements and rotations considering the first-order Shear deformation theory (FSDT). The nonlinear governing equations are solved using the differential quadrature method (DQM) which is a highly accurate numerical method and a new semi-analytical polynomial method (SAPM). The ordinary differential equations (ODE's) are converted to the nonlinear algebraic equations applying DQM or SAPM. Then, the Newton–Raphson iterative scheme is applied. The obtained results of DQM and SAPM are compared. It is concluded that although, the SAPM's formulation is considerably simple in comparison with DQM, however, the results of two methods are so close to each other. The results are validated with available researches. The effects of small scale parameter, the value of van der Waals interaction between the layers, different values of elastic foundation and loading, the comparison between the local and nonlocal deflections and linear to nonlinear analysis are investigated.

Keywords : Bilayer orthotropic annular/circular graphene sheets; Eringen nonlocal elasticity theory; Winkler-Pasternak elastic foundation; Differential quadrature method (DQM) ; Semi analytical polynomial method (SAPM).

1 INTRODUCTION

GRAPHENE sheets are layers of carbon atoms that are arranged in hexagon forms frequently and regularly and lead to extraordinary mechanical, thermal and electrical properties and the high stiffness to inertia ratio. These significant properties motivate researchers to employ them within other substances. So, analysis of mechanical properties of nanostructures is considerable.

In recent years, many researchers are persuaded to study the mechanical behavior of nano-structures using experimental, molecular simulation and continuum mechanics methods. The experimental method has two major restrictions. First, expensive laboratory tools and the second, loading restrictions. Only the axial loading can be applied in experimental works. In this case, it can be possible to mention a methodology which was presented by Androulidakis et al [1] for deriving true experimental axial stress–strain curves in both tension and compression for monolayer graphene. According to the vast computational expenses of nano-structures analyses when using atomic

*Corresponding author. Tel.: +985136625046.
E-mail address: jabbarzadeh@mshdiau.ac.ir (M. Jabbarzadeh).

lattice dynamics and molecular dynamic simulations, there is a great interest in applying continuum mechanics for analysis of such structures. Comparison between Classical theories in elasticity and the obtained results from experimental tasks shows that using of the classical elasticity theory leads to considerable differences between results. In recent years various size dependent continuum theories are introduced such as couple stress theory [2], strain gradient elasticity theory [3-5], modified couple stress theory [5-8] and nonlocal elasticity theory [10-12]. These theories are comprised of information about the inter-atomic forces and internal lengths that is introduced as small scale effect in nonlocal elasticity theory [13]. Through these methods, the Eringen nonlocal elasticity theory [11] has been used much more than the others. In this theory, the stress at a reference point is a function of the strain field at every point in the body. Anjomshoa et al [14] investigated Frequency analysis of embedded orthotropic circular and elliptical micro/nano-plates using nonlocal variational principle. They proved that the natural frequencies depend on the non-locality of the micro/nano-plate, especially at small dimensions. Kitipornchai et al. [15] used the continuum plate model for mechanical analysis of graphene sheets. He et al. [16] described van der Waals interaction between the layers of multilayered graphene sheets by an explicit formula based on the continuum mechanics and a multiple-elastic beam model. Liew et al. [17] studied the vibration behavior of multilayered graphene sheets resting on an elastic matrix based on a continuum-based plate model. Ghorbanpour Arani et al [18] applied nonlocal DQM for large amplitude vibration of annular boron nitride sheets on nonlinear elastic medium. They concluded that with increasing nonlocal parameter, the frequency of the coupled system becomes lower. Scarpa et al. [19] studied both circular and rectangular graphene sheets subjected to point loading based on a special equivalent atomistic-continuum model. They found that the rectangular SLGSs show a different distribution of the geometrical and mechanical properties, compared to the circular configuration. Murmu and Pradhan [20] developed a single elastic beam model for thermo-mechanical vibration of a single-walled carbon nanotube resting on an elastic medium based on the nonlocal elasticity theory. Ke et al. [21] investigated the nonlinear free vibration of embedded double-walled carbon nanotubes based on the Eringen's nonlocal elasticity theory and von Karman geometric nonlinearity using differential quadrature method. Nonlinear free vibrations of a nano-beam with simply supported boundary conditions was studied by Dong and Lim [22] based on nonlocal elasticity theory. Ansari et al. [23] investigated the vibrational characteristics of multilayered Graphene sheets with different boundary conditions embedded in an elastic medium using finite element method. Pradhan and Phadikar [24] studied vibration analysis of multilayered graphene sheets embedded in polymer matrix by using the nonlocal continuum mechanics. Pradhan and Kumar [25] investigated the small scale effect on the vibration analysis of orthotropic single layered graphene sheets resting on a Winkler-type and Pasternak-type elastic foundation. Nonlinear free vibration of single-walled carbon nanotubes based on the Timoshenko beam model was studied by Yang et al. [27]. Shen et al. [27] studied nonlinear vibration behavior for a simply supported single layer graphene sheet in thermal environments in order to obtain the nonlocal parameter. The nonlinear bending analysis of single-layered graphene sheets has been investigated by Golmakani and Rezatalab [28]. They proved that the maximum deflection decreases along the increase of nonlocal parameter and also the local and nonlocal elasticity theories were compared. Mohammadi et al [29] studied small scale effect on the vibration of orthotropic plates embedded in an elastic medium and under biaxial in-plane pre-load via nonlocal elasticity theory. Their results are shown that with the decrease of in-plane pre-loads the curves isotropic and orthotropic non-dimensional frequency in approaches close to each other.

In present study, solutions for nonlinear bending analysis of bilayer orthotropic circular/annular graphene sheets are obtained based on the FSDT nonlocal elasticity theory. The DQM and a new semi-analytical polynomial method (SAPM) are used to solve the governing equations. To demonstrate the accuracy of obtained results, the results are validated with available literatures. Besides, the effect of nonlocal parameter on deflection, the effects of different parameters such as linear to nonlinear analysis, the value of van der Waals interaction between the layers, nonlocal to local deflection ratio and different types of boundary conditions are investigated.

2 GOVERNING EQUATIONS

The geometry of a radially bilayer annular/circular graphene sheet is shown in Fig.1 with thickness *h*, inner radius r_i, outer radius r_o, under uniform transverse loading *q* that is rested on two parameters Winkler-Pasternak elastic matrix. k_w and k_p are the Winkler and Pasternak stiffness coefficients of elastic foundation respectively. The term $k_o(w_2 - w_1)$ refers to the van der Waals interaction bonds between the layers in Fig. 1(b). k_o is the van der Waals stiffness. According to the first-order shear deformation theory of plates, the displacements field can be expressed as

follows [35]. (The index *i* identifies the layers. *i=1* refers to the upper layer under transverse load and *i=2* to the bottom layer that is rested on elastic foundation)

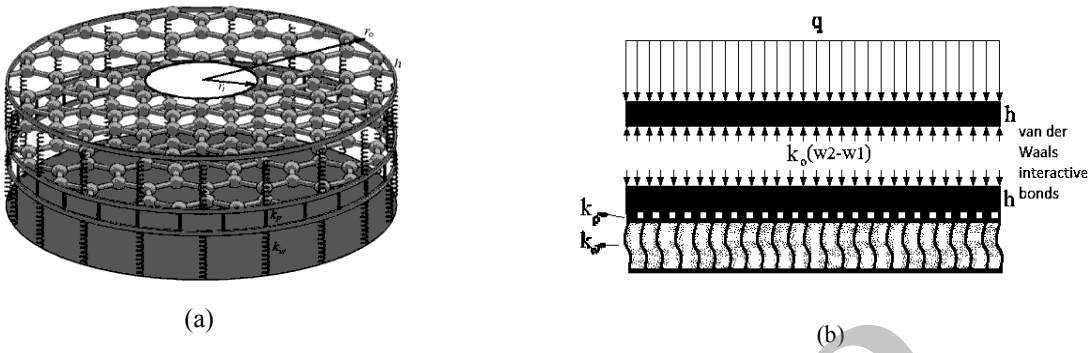

(a) (b)

Fig.1
Figure of bilayer annular graphene sheet (a) perspective (b) front plane view.

$$Ui(r,z) = ui(r) + z\,\psi i(r) \tag{1}$$

$$Vi(r,z) = 0 \tag{2}$$

$$Wi(r) = wi(r) \tag{3}$$

The first-order shear deformation theory implies a linear displacement variation through the thickness. The shear strain, and hence the shear stress, across the thickness of the plate is not neglected in this theory. However, the shear strain is constant across the thickness of the plate. By considering this assumption, the obtained results would have small difference with precise results, since the shear stress is known to be parabolic even for simple plate geometries. To account for the inaccuracy in the shear strain, a shear correction factor (κ_s) is applied so that the correct amount of internal energy is predicted by the theory. u and w are the displacement components of the mid-plane along the r and z directions respectively. Also ψ denotes the rotational function of the transverse normal about θ axis. The graphene sheet is assumed to have large amplitude deformation, so the von Karman type strain–displacement relations are used as [36]:

$$\varepsilon i_r = \frac{dui}{dr} + z\,\frac{d\psi i}{dr} + \frac{1}{2}\left(\frac{dwi}{dr}\right)^2 \tag{4}$$

$$\varepsilon i_\theta = \frac{ui}{r} + z\,\frac{\psi i}{r} \tag{5}$$

$$\gamma i_{rz} = \frac{dwi}{dr} + \psi i \tag{6}$$

where εi_r and εi_θ are the normal strains and γi_{rz} is the shear strain. In nonlocal elasticity theory, the effects of small scale and atomic forces come directly to the constitutive equations as material parameters [10]. Eringen presented a differential form of the nonlocal constitutive equation from nonlocal balance law as follow [12, 13]:

$$\left(1-\mu\nabla^2\right)\sigma^{NL}=\sigma^{L}=C:\varepsilon,\mu=\left(e_0a\right)^2$$

$$C=\begin{bmatrix}\dfrac{E_r}{1-\nu_{r\theta}\nu_{\theta r}} & \dfrac{\nu_{r\theta}E_\theta}{1-\nu_{r\theta}\nu_{\theta r}} & 0\\ 0\dfrac{\nu_{r\theta}E_\theta}{1-\nu_{r\theta}\nu_{\theta r}} & \dfrac{E_\theta}{1-\nu_{r\theta}\nu_{\theta r}} & 0\\ 0 & 0 & G_{rz}\end{bmatrix} \tag{7}$$

In which a is the internal characteristic length and e_0 is the material constant which is defined by experiment. The parameter (e_0a) is the small-scale parameter revealing the small-scale effect on the responses of nano-size structures. The value of the small-scale parameter depends on boundary condition, chirality, mode shapes, number of walls, and the nature of motions [12]. The nonlocal stresses can be defined by considering Eq. (7) as follows [12]:

$$\left(\sigma i_r^{NL}-\mu\left(\nabla^2\sigma i_r^{NL}-\frac{2}{r^2}\left(\sigma i_r^{NL}-\sigma i_\theta^{NL}\right)\right)\right)=\sigma i_r^{L} \tag{8}$$

$$\left(\sigma i_\theta^{NL}-\mu\left(\nabla^2\sigma i_\theta^{NL}+\frac{2}{r^2}\left(\sigma i_r^{NL}-\sigma i_\theta^{NL}\right)\right)\right)=\sigma i_\theta^{L} \tag{9}$$

$$\left(\sigma i_{rz}^{NL}-\mu\left(\nabla^2\sigma i_{rz}^{NL}-\frac{1}{r^2}\sigma i_{rz}^{NL}\right)\right)=\sigma i_{rz}^{L} \tag{10}$$

Also, ∇^2 is the Laplacian operator as follow:

$$\nabla^2=\frac{d^2}{dr^2}+\frac{1}{r}\frac{d}{dr} \tag{11}$$

The nonlocal force, moment ($Ni_j^{NL}, Mi_j^{NL}\left(j=r,\theta\right)$) and shear force Qi_r^{L} components are expressed as follows [36]:

$$(Ni_r,Ni_\theta,Qi_r)^{NL}=\int_{-\frac{h}{2}}^{\frac{h}{2}}\left(\sigma i_r,\sigma i_\theta,\kappa_s\sigma i_{rz}\right)^{NL}dz \tag{12}$$

$$(Mi_r,Mi_\theta)^{NL}=\int_{-\frac{h}{2}}^{\frac{h}{2}}\left(\sigma i_r,\sigma i_\theta\right)^{NL}zdz \tag{13}$$

As mentioned before, κ_s denotes the transverse shear correction coefficient ($\kappa_s=5/6$). By substituting Eqs. (8-10) into Eqs. (12, 13) the nonlocal force, moment and shear force components can be defined as follows:

$$\left(Ni_r^{NL}-\mu\left(\nabla^2Ni_r^{NL}-\frac{2}{r^2}\left(Ni_r^{NL}-Ni_\theta^{NL}\right)\right)\right)=Ni_r^{L} \tag{14}$$

$$\left(Ni_\theta^{NL}-\mu\left(\nabla^2Ni_\theta^{NL}+\frac{2}{r^2}\left(Ni_r^{NL}-Ni_\theta^{NL}\right)\right)\right)=Ni_\theta^{L} \tag{15}$$

$$\left(Mi_r^{NL}-\mu\left(\nabla^2 Mi_r^{NL}-\frac{2}{r^2}\left(Mi_r^{NL}-Mi_\theta^{NL}\right)\right)\right)=Mi_r^{L} \tag{16}$$

$$\left(Mi_\theta^{NL}-\mu\left(\nabla^2 Mi_\theta^{NL}+\frac{2}{r^2}\left(Mi_r^{NL}-Mi_\theta^{NL}\right)\right)\right)=Mi_\theta^{L} \tag{17}$$

$$\left(Qi_r^{NL}-\mu\left(\nabla^2 Qi_r^{NL}-\frac{2}{r^2}\left(Qi_r^{NL}\right)\right)\right)=Qi_r^{L} \tag{18}$$

$Ni_j^L, Mi_j^L\ (j=r,\theta)$ and Qi_r^L are the local in-plane force, moment and the shear force resultants which are defined for orthotropic material as:

$$Mi_r^{L}=\frac{h^3}{12\left(1-\nu_{r\theta}\nu_{\theta r}\right)}\left(E_r\frac{d\psi i}{dr}+\frac{E_\theta\nu_{r\theta}}{r}\psi i\right) \tag{19}$$

$$Mi_\theta^{L}=\frac{E_\theta h^3}{12\left(1-\nu_{r\theta}\nu_{\theta r}\right)}\left(\nu_{r\theta}\frac{d\psi i}{dr}+\frac{\psi i}{r}\right) \tag{20}$$

$$Ni_r^{L}=\frac{h}{\left(1-\nu_{r\theta}\nu_{\theta r}\right)}\left(E_r\left(\frac{dui}{dr}+\frac{1}{2}\left(\frac{dwi}{dr}\right)^2\right)+\nu_{r\theta}E_\theta\left(\frac{ui}{r}\right)\right) \tag{21}$$

$$Ni_\theta^{L}=\frac{E_\theta h}{\left(1-\nu_{r\theta}\nu_{\theta r}\right)}\left(\nu_{r\theta}\left(\frac{dui}{dr}+\frac{1}{2}\left(\frac{dwi}{dr}\right)^2\right)+\frac{ui}{r}\right) \tag{22}$$

$$Qi_r^{L}=\kappa_s G_{rz}h\left(\frac{dwi}{dr}+\psi i\right) \tag{23}$$

Using the principle of stationary total potential energy, the governing equations as well as the related boundary conditions along the edges of annular plate can be obtained. The equations of the total potential energy in case of nonlocal form are expressed below [18]:

$$\delta\Pi=\delta Ui+\delta\Omega i=0 \tag{24}$$

$$\delta Ui=\iiint_v\left(\sigma i_r^{NL}\delta\varepsilon i_r+\sigma i_\theta^{NL}\delta\varepsilon i_\theta+\kappa_s\sigma i_{rz}^{NL}\delta\gamma i_{rz}\right)dV \tag{25}$$

$$\delta\Omega 1=\int_{r_i}^{r_o}\int_0^{2\pi}\left(q+k_o\left(w_2-w_1\right)\right)\delta w r dr d\theta \quad \text{Upper layer} \tag{26}$$

$$\delta\Omega 2=\int_{r_i}^{r_o}\int_0^{2\pi}\left(-k_o\left(w_2-w_1\right)-k_w w_2+k_p\nabla^2 w_2\right)\delta w r dr d\theta \quad \text{Bottom layer} \tag{27}$$

where δ is the variation symbol, U and Ω are the strain energy and potential of applied forces respectively. By using the nonlocal stress resultants (12, 13) and the relations between the stress resultants in local and nonlocal forms (14-18), the equilibrium equations of annular/circular graphene sheet cylindrical coordinates system are obtained as:

$$\delta u_i : Ni^L_{r,r} + \frac{1}{r}\left(Ni^L_r - Ni^L_\theta\right) = 0 \qquad i = 1,2 \tag{28}$$

$$\delta w_1 : Q1_{r,r} + \frac{1}{r}Q1_r + \left(1-\mu\nabla^2\right)\left(q + k_o\left(w_2 - w_1\right) + N1_r\frac{1}{r}\frac{dw_1}{dr} + N1_{r,r}\frac{dw_1}{dr} + N1_r\frac{d^2w_1}{dr^2}\right) = 0 \text{ Upper layer} \tag{29}$$

$$\delta w_2 : Q2_{r,r} + \frac{1}{r}Q2_r + \left(1-\mu\nabla^2\right)\left(k_p\nabla^2 w_2 - k_w w_2 - k_o\left(w_2 - w_1\right) + N2_r\frac{1}{r}\frac{dw_2}{dr} + N2_{r,r}\frac{dw_2}{dr} + N2_r\frac{d^2w_2}{dr^2}\right) = 0 \text{ Bottom layer} \tag{30}$$

$$\delta\psi_i : Mi^L_{r,r} + \frac{1}{r}\left(Mi^L_r - Mi^L_\theta\right) - Qi^L_r = 0 \qquad i = 1,2 \tag{31}$$

For sake of generality and convenience, the following non-dimensional terms are introduced:

$$r^* = \frac{r}{r_o};\ z^* = \frac{z}{h};\ u_i^* = \frac{u_i}{h};w_i^* = \frac{w_i}{r_o};\psi_i^* = \psi_i;\eta = \frac{h}{r_o};\ q^* = \frac{q}{E_r};\mu^* = \frac{\mu}{r_o^2}$$

$$k_w^* = \frac{k_w r_o}{E_r};k_p^* = \frac{k_p}{E_r h};\nabla^{*2} = \frac{d^2}{dr^{*2}} + \frac{1}{r^*}\frac{d}{dr^*};\nabla^2 = \frac{\nabla^{*2}}{r_o^2};\rho 1 = \frac{E_\theta}{E_r};\rho 2 = \frac{G_{rz}}{E_r};\upsilon = 1 - \nu_{r\theta}\nu_{\theta r}$$

Substituting Eqs. (19-23) in dimensionless form into Eqs. (28-31) gives the equilibrium equations. The Eq. (33) is presented for the upper layer under the uniform transverse load.

$$\left(\frac{\eta\rho 1}{\upsilon}\right)\left(\nu_{r\theta}\left(\frac{dui^*}{dr^*} + \frac{1}{2\eta}\left(\frac{dwi^*}{dr^*}\right)^2\right) + \frac{ui^*}{r^*}\right) - \left(\frac{\eta}{\upsilon}\right)\left(\frac{dui^*}{dr^*} + \frac{1}{2\eta}\left(\frac{dwi^*}{dr}\right)^2 + \nu_{r\theta}\rho 1\left(\frac{ui^*}{r^*}\right)\right)$$
$$-r^*\left(\left(\frac{\eta}{\upsilon}\right)\left(\frac{d^2ui^*}{dr^{*2}} + \frac{1}{\eta}\left(\frac{dwi^*}{dr^*}\right)\left(\frac{d^2wi^*}{dr^{*2}}\right) + \nu_{r\theta}\rho 1\left(-\frac{ui^*}{r^{*2}} + \frac{1}{r^*}\frac{dui^*}{dr^*}\right)\right)\right) = 0 \tag{32}$$

$$\kappa_s\rho 2\left(\frac{d^2w1^*}{dr^{*2}} + \frac{d\psi 1^*}{dr^*} + \frac{1}{r^*}\frac{dw1^*}{dr^*} + \frac{\psi 1^*}{r^*}\right) + \frac{q}{E_r\eta} + \left(\frac{\eta\rho 1}{r^*\upsilon}\right)\left(\nu_{r\theta}\left(\frac{du1^*}{dr^*} + \frac{1}{2\eta}\left(\frac{dw1^*}{dr^*}\right)^2\right) + \frac{dw1^*}{dr^*}\right)\left(\frac{dw1^*}{dr^*}\right) + \left(\frac{\eta}{\upsilon}\right)$$
$$\left(\frac{du1^*}{dr^*} + \frac{1}{2\eta}\left(\frac{dw1^*}{dr^*}\right)^2 + \nu_{r\theta}\rho 1\frac{u1^*}{r^*}\right)\left(\frac{d^2w1^*}{dr^{*2}}\right) + \frac{k_o r_o\left(w2^* - w1^*\right)}{E_r\eta} - \frac{\mu}{r_o^2}\left(\frac{h}{r_o\upsilon}\left(\frac{d^3u1^*}{dr^{*3}} + \frac{1}{\eta}\left(\left(\frac{dw1^*}{dr^*}\right)^2 + \left(\frac{dw1^*}{dr^*}\right)\left(\frac{d^3w1^*}{dr^{*3}}\right)\right)\right)\right.$$
$$+\frac{\nu_{r\theta}\rho 1}{r^*}\left(\frac{d^2u1^*}{dr^{*2}} + \frac{2}{r^*}\frac{du1^*}{dr^*} + \frac{2u1^*}{r^{*2}}\right)\frac{d^2w1^*}{dr^{*2}}\Bigg) + \frac{2h}{r_o\upsilon}\left(\frac{d^2u1^*}{dr^{*2}} + \frac{1}{\eta}\left(\frac{dw1^*}{dr^*}\right)\left(\frac{d^2w1^*}{dr^{*2}}\right) + \frac{\nu_{r\theta}\rho 1}{r^*}\left(\frac{du1^*}{dr^*} - \frac{u1^*}{r^*}\right)\right)\frac{d^3w1^*}{dr^{*3}} +$$
$$\frac{h}{r_o\upsilon}\left(\frac{du1^*}{dr^*} + \frac{1}{2\eta}\left(\frac{dw1^*}{dr^*}\right)^2 + \frac{\nu_{r\theta}\rho 1u1^*}{r^*}\right)\frac{d^4w1^*}{dr^{*4}} + \frac{2h\rho 1}{r^{*3}r_o\upsilon}\left(\nu_{r\theta}\left(\frac{du1^*}{dr^*} + \frac{1}{2\eta}\left(\frac{dw1^*}{dr^*}\right)^2\right) + \frac{u1^*}{r^*}\right)\frac{dw1^*}{dr^*} - \frac{2h\rho 1}{r^{*2}r_o\upsilon}$$
$$\left(\nu_{r\theta}\left(\frac{d^2u1^*}{dr^{*2}} + \frac{1}{\eta}\left(\frac{dw1^*}{dr^*}\right)\left(\frac{d^2w1^*}{dr^{*2}}\right)\right) + \frac{1}{r^*}\left(\frac{du1^*}{dr^*} - \frac{u1^*}{r^*}\right)\right)\frac{dw1^*}{dr^*} - \frac{2h\rho 1}{r^{*2}r_o\upsilon}\left(\nu_{r\theta}\left(\frac{du1^*}{dr^*} + \frac{1}{2\eta}\left(\frac{dw1^*}{dr^*}\right)^2\right) + \frac{u1^*}{r^*}\right)\frac{d^2w1^*}{dr^{*2}}$$
$$+\frac{h\rho 1}{r^*r_o\upsilon}\left(\nu_{r\theta}\left(\frac{d^3u1^*}{dr^{*3}} + \frac{1}{\eta}\left(\left(\frac{d^2w1^*}{dr^{*2}}\right)^2 + \left(\frac{dw1^*}{dr^*}\right)\left(\frac{d^3w1^*}{dr^{*3}}\right)\right)\right) + \frac{1}{r^*}\frac{d^2u1^*}{dr^{*2}} - \frac{2}{r^{*2}}\frac{du1^*}{dr^*} + \frac{u1^*}{r^{*3}}\right)\frac{dw1^*}{dr^*} + \frac{2h\rho 1}{r^*r_o\upsilon} \tag{33}$$

$$\left(\nu_{r\theta}\left(\frac{d^2u1^*}{dr^{*2}}+\frac{1}{\eta}\left(\frac{dw1^*}{dr^*}\right)\left(\frac{d^2w1^*}{dr^{*2}}\right)\right)+\frac{1}{r^*}\frac{du1^*}{dr^*}-\frac{u1^*}{r^{*2}}\right)\frac{d^2w1^*}{dr^{*2}}+\frac{h\rho1}{r^*r_o\upsilon}\left(\nu_{r\theta}\left(\frac{du1^*}{dr^*}+\frac{1}{2\eta}\left(\frac{d^2w1^*}{dr^{*2}}\right)^2\right)+\frac{u1^*}{r^*}\right)\frac{d^3w1^*}{dr^{*3}}$$
$$-\frac{k_or_o}{E_r\eta}\left(\frac{d^2w2^*}{dr^{*2}}-\frac{d^2w1^*}{dr^{*2}}\right)+\frac{1}{r^*}\left(\frac{h}{r_o\upsilon}\left(\frac{d^2u1^*}{dr^{*2}}+\frac{1}{\eta}\left(\frac{dw1^*}{dr^*}\right)\left(\frac{d^2w1^*}{dr^{*2}}\right)+\frac{\nu_{r\theta}\rho1}{r^*}\left(\frac{du1^*}{dr^*}-\frac{u1^*}{r^*}\right)\right)\frac{d^2w1^*}{dr^{*2}}+\frac{h}{r_o\upsilon}\right.$$
$$\left(\frac{du1^*}{dr^*}+\frac{1}{2\eta}\left(\frac{d^2w1^*}{dr^{*2}}\right)^2+\nu_{r\theta}\rho1\left(\frac{u1^*}{r^*}\right)\right)\frac{d^3w1^*}{dr^{*3}}-\frac{h\rho1}{r^{*2}r_o\upsilon}\left(\nu_{r\theta}\left(\frac{du1^*}{dr^*}+\frac{1}{2\eta}\left(\frac{dw1^*}{dr^*}\right)^2\right)+\frac{u1^*}{r^*}\right)\frac{dw1^*}{dr^*}+ \quad (33)$$
$$\frac{h\rho1}{r^*r_o\upsilon}\left(\nu_{r\theta}\left(\frac{d^2u1^*}{dr^{*2}}+\left(\frac{1}{\eta}\left(\frac{dw1^*}{dr^*}\right)\left(\frac{d^2w1^*}{dr^{*2}}\right)\right)+\frac{1}{r^*}\left(\frac{du1^*}{dr^*}-\frac{u1^*}{r^*}\right)\right)\frac{dw1^*}{dr^*}+\right.$$
$$\left.\left.\frac{h\rho1}{r^*r_o\upsilon}\left(\nu_{r\theta}\left(\frac{du1^*}{dr^*}+\frac{1}{2\eta}\left(\frac{dw1^*}{dr^*}\right)^2\right)+\frac{u1^*}{r^*}\right)\frac{d^2w1^*}{dr^{*2}}-\frac{k_or_o}{E_r\eta}\left(\frac{dw2^*}{dr^*}-\frac{dw1^*}{dr^*}\right)\right)\right)=0$$

$$\frac{\eta^2}{12\upsilon}\left(\frac{d^2\psi i^*}{dr^{*2}}+\nu_{r\theta}\rho1\left(\frac{d\psi i^*}{dr^*}-\frac{\psi i^*}{r^*}\right)\right)+\frac{1}{12r^*}\frac{\eta^2}{\upsilon}\left(\left(\frac{d\psi i^*}{dr^*}-\frac{\nu_{r\theta}\rho1\psi i^*}{r^*}\right)-\rho1\left(\frac{\psi i^*}{r^*}+\nu_{r\theta}\left(\frac{d\psi i^*}{dr^*}\right)\right)\right)-\kappa_s\rho2\left(\frac{dwi^*}{dr^*}+\psi i^*\right)=0 \quad (34)$$

3 SOLUTION

Two methods are applied to solve the obtained governing equations. First, the DQ that is a highly accurate numerical method is used as many researchers have used this method in their researches. Also, a new semi-analytical polynomial method (SAPM) is introduced by authors. SAPM has all the premiums of DQM such as remarkable accuracy and high rate of convergence and does not have the DQM's weaknesses.

3.1 Differential quadrature method (DQM)

First, the differential quadrature method (DQM) is used to solve the equilibrium equations for different boundary conditions. The DQM was proposed by Bellman and coworkers for solving differential equations [30-31]. This method is highly accurate, convenient and capable to solve the partial differential equations, so, many researchers have used the DQM to analyze the sets of ordinary and partial differential equations system. In this method, the derivatives of a function at any grid points is approximated using weighted sum of all the functional values at certain points in the whole computational domain.

Using the DQM, derivatives of a function *f(r)* at point *r* can be defined as following linear sum of the function values:

$$\left.\frac{d^{(n)}f}{dr^{(n)}}\right|_{r_i}=\sum_{j=1}^{N}A_{ij}^{(n)}f(r_i)\quad i=1,...,N \quad (35)$$

$$A_{ij}^{(n)}=n\left[A_{ij}^{(1)}A_{ii}^{(n-1)}-\frac{A_{ij}^{(n-1)}}{\left(r_i-r_j\right)}\right]\ i\neq j, A_{ii}^{(n)}=-\sum_{j=1,\neq i}^{N}A_{ij}^{(n)}\quad i,j=1...N \quad (36)$$

In which, *N* is the number of grid points along *r* direction. It is more offered to use the grid point distribution

which is based on Gauss-Chebyshev-Lobatto points to gain more accurate results [28]. According to the Gauss-Chebyshev-Lobatto grid point's distribution, the coordinates of the grid points are as follow:

$$r_i = \frac{(r_i + r_o)}{2} - \cos\left(\left(\frac{i-1}{N-1}\right)\pi\right)\left(\frac{(r_o - r_i)}{2}\right) \quad i = 1...N \tag{37}$$

Using the DQM, the set of differential equations is converted to nonlinear algebraic equations system. Now, this system can be solved by using several numerical methods such as Fixed Point or Newton-Raphson Method. In this paper, because of considerable accuracy and high rate of convergence, the Newton-Raphson method is applied.

3.2 Semi analytical polynomial method (SAPM)

The SAPM which is innovated by authors, is an extremely simple method for solving the ordinary and partial differential equations based on the definition of polynomials. Some of the privileges of this method can be classified as follows:

- The formulation is considerably simpler than DQM.
- The accuracy is the same as DQM.
- Computer programming is extremely simpler and the processing time is shorter in comparison with DQM.

Formulation is presented for solving the ordinary differential equations. Consider a general ordinary differential equation as follow:

$$g_1(r)\frac{df(r)}{dr} + g_2(r)\frac{d^2 f(r)}{dr^2} + ... + g_n(r)\frac{d^n f(r)}{dr^n} + h(r) = 0, \quad r_i \le r \le r_o \tag{38}$$

The domain $r_i \le r \le r_o$ is divided to *N* grid point. The function *f(x)* is defined in presented method as follow:

$$f(r) = \sum_{i=1}^{N} a_i r^{(i-1)} \quad r_i \le r \le r_o \tag{39}$$

Substituting Eq. (39) into Eq. (38) the differential equation will be converted to algebraic equation as follow:

$$g_1(r)\frac{d}{dr}\left(\sum_{i=1}^{N} a_i r^{(i-1)}\right) + g_2(r)\frac{d^2}{dr^2}\left(\sum_{i=1}^{N} a_i r^{(i-1)}\right) + ... + g_n(r)\frac{d^n}{dr^n}\left(\sum_{i=1}^{N} a_i r^{(i-1)}\right) + h(r) = 0, \quad r_i \le r \le r_o \tag{40}$$

For an *n* order differential equation, it is needed the number of (*n*) boundary conditions in boundary points r_i and r_o. For example in a second order differential equation the value of function *f(x)* or derivation *f(r)* must be known in boundaries (dark points in Fig. 2.). Consequently, two algebraic equations in boundaries would be determined and the rest of algebraic equations can be derived from Eq. (40) in inner grid points (bright points in Fig. 2.).

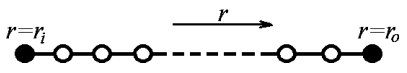

Fig.2
The division of one directional domain for ODE problems.

Now there are a set of (*N*) algebraic equations and (*N*) unknown constants $a_i, i = 1..N$. The constants a_i should be substituted in Eq. (38), then the function *f(r)* will be determined. This is one of the simplest methods for solving the ordinary differential equations. The main concept of SAPM can be illustrated in Flowchart .1.

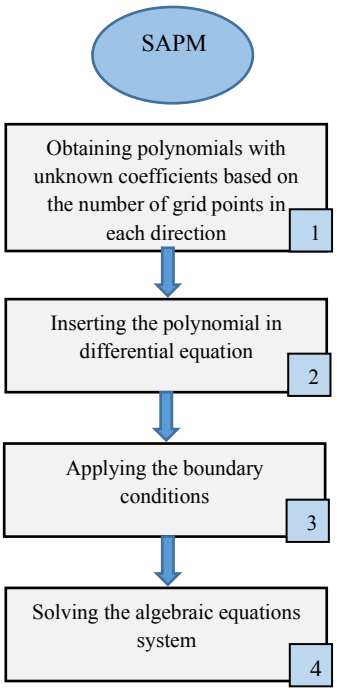

Flowchart 1
Procedure of computation for SAPM.

If there is a set of ordinary differential equations, the procedure is similar to the mentioned explanation. Now, according to the mentioned procedures for SAPM, the functions u^*, w^* and ψ^* can be introduced below:

$$u^* = a_1 + a_2 r + a_3 r^2 + ... + a_N r^{(N-1)} \tag{41}$$

$$w^* = a_{N+1} + a_{N+2} r + a_{N+3} r^2 + ... + a_{2N} r^{(N-1)} \tag{42}$$

$$\psi^* = a_{2N+1} + a_{2N+2} r + a_{2N+3} r^2 + ... + a_{3N} r^{(N-1)} \tag{43}$$

Now by substituting u^*, w^* and ψ^* as polynomial functions into Eqs. (32-34), the differential equations are converted to algebraic equations that can be solved by use of a numerical method such as Newton-Raphson method.

4 BOUNDARY CONDITIONS

In this paper, the boundary conditions are considered for the simply supported (S), clamped (C) and free (F) edges in $r = r_i, r_o$. So, the plate can be defined with two boundaries in $r = r_i, r_o$ as CC, SS, FS, FC and etc. The first letter refers to the boundary condition at $r = r_i$ and the second one at $r = r_o$. (Fig. 3.)

$$S: ui = wi = Mi_r = 0 \quad , \quad C: ui = wi = \psi i = 0 \quad , \quad F: Qi_r = Mi_r = Ni_r = 0 \qquad (r = r_i, r_o)$$

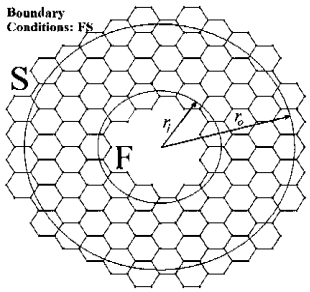

Fig.3
Definition of boundary conditions.

5 NUMERICAL RESULTS

First, it is considered a single layer annular graphene sheet to check the rate of convergence of DQM and SAPM. Fig. 4. shows that the desirable results are obtained with only nine grid points along the r direction. Also, it is proved that the accuracy of SAPM method is similar to DQM, whereas SAPM is extremely simpler and faster. The material properties of the plate are as follows: $r_i / r_o = 0.2; h = 0.34\text{nm}$

$E_r = 1.06\times10^{12}\,\text{Pa}; E_\theta = 0.85\times10^{12}\,\text{Pa};\ \nu_{r\theta}=\nu_{\theta r}=0.3; q^* = 10^8 / E; k_w = 1.13\text{GPa/nm}; k_p = 0; k_p = 1.13\text{Pa.m}; k_0 = 0$

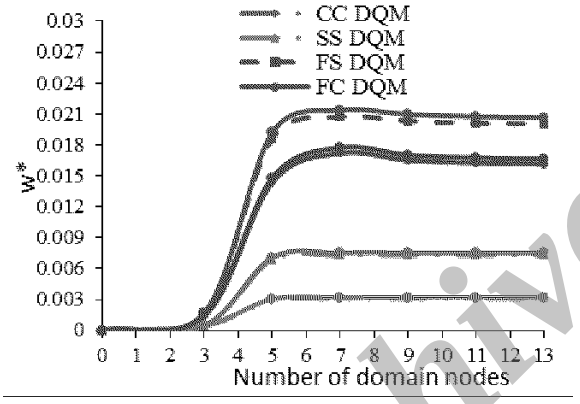

Fig.4
Variation of dimensionless deflection versus the number of grid points for DQM and SAPM domain.

Since there are not any papers in nonlinear bending of bilayer annular/circular graphene sheets, the local elasticity theory is considered and the central deflection of an single layer annular plate under uniform transverse load is compared with references [32-34] in Table 1.

$\nu_{r\theta}=\nu_{\theta r} = 0.3; R^* = r_o / h=10; E_r = E_\theta = 2\times10^6\,\text{Pa}; \mu=0$

Table 1
Comparison dimensionless deflection $w^* = \left(64Eh^3\right)W / \left(12q\left(1-\nu^2\right)r_o^4\right)$ with the other references for circular plate.

	w^*			
$q^* = \frac{q}{E}$	[32]	[33]	[34]	Present Paper
0.0001	0.1678	0.1687	0.1706	0.168
0.0003	0.4583	0.4655	0.5119	0.4588
0.001	1.0509	1.0937	1.7069	1.0514

Also, the results are compared with references [35, 36] for an annular plate in Table 2. The material properties of the plate are as follows: $\nu_{r\theta}=\nu_{\theta r} = 0.288; R^*=r_o / h=0.15; E_r = E_\theta = 280\text{GPa}; \mu=0$

Table 2

Comparison dimensionless deflection $w^* = \left(64Eh^3\right)W / \left(12q\left(1-\nu^2\right)r_o^4\right)$ with the other references for annular plate.

w^*					
[35]		[36]		Present study	
Clamped	Simply Supported	Clamped	Simply Supported	Clamped	Simply Supported
2.781	10.623	2.774	10.572	2.803	10.567

In this paper, in addition to FSDT analysis, the governing equations are derived based on the classical plate theory (CLPT) considering nonlinear strain fields. Comparison between FSDT and CLPT analysis is shown in Table 3. with clamped edges and the material properties as follows:

$r_i / r_o = 0.2; h = 0.34\text{nm}; E_r = 1.06\times10^{12}\,\text{Pa}; E_\theta = 0.85\times10^{12}\,\text{Pa}; \nu_{r\theta}=\nu_{\theta r}=0.3; q^* = 10^8 / E; k_w = 1.13\text{GPa/nm}; k_p = 1.13\text{Pa.m}$

It is observed that the descending procedure of the deflection versus the increase of nonlocal parameter for CLPT analysis is similar to FSDT. On the other hand, with increase of nonlocal parameter the deflection decreases for both CLP and FSD theories. In addition, the difference between the results of two theories decreases with increase of small scale effects.

Table 3

Comparison between CLPT and FSDT analysis

w^*			
$e_0a\,(\text{nm})$	FSDT	CLPT	FSDT/CLPT
0	0.003063	0.003380	0.906
0.5	0.002985	0.003289	0.907
1	0.002774	0.003044	0.911
1.5	0.002484	0.002713	0.915
2	0.002170	0.002359	0.920

Also, the comparison between the deflection of single layer and bilayer sheets is shown in Table 4. for SS boundary conditions. The deflection of the upper layer is given for the bilayer sheet. It is concluded that with rise of k_o the maximum deflection and the effect of nonlocal parameter decreases and also, the variation of the ratio $w^*_{k_o} / w^*_{\text{Single layer}}$ increases.

Table 4

Comparison the results of single layer and bilayer sheets.

w^*					
$e_0a\,(\text{nm})$	Single layer	Bilayer		$\frac{w^*_{k_o=2\text{GPa/nm}}}{w^*_{\text{Single layer}}}$	$\frac{w^*_{k_o=50\text{GPa/nm}}}{w^*_{\text{Single layer}}}$
		k_o = 2 (GPa/nm)	k_o = 50 (GPa/nm)		
0	0.0145	0.00974	0.00773	0.67	0.53
1	0.0136	0.00900	0.00760	0.68	0.57
1.5	0.0125	0.00848	0.00745	0.69	0.60
2	0.0115	0.00803	0.00728	0.70	0.63

Sample 1: Bilayer annular plate

A bilayer annular graphene sheet is considered. the variation of dimensionless deflection versus van der Waals interaction between the layers is shown in Fig. 5(a) for SS boundary conditions and (b) for CC (e0a=1nm). The van der Waals interaction between the layers is an obstacle for increase of the upper layer's defection (Eq. (29), Fig. 1(b)). Consequently, with rise of k_o, the maximum deflection of the upper layer decreases. On the contrary, the deflection of bottom layer is increased. Totally, the two deflection of upper and bottom layer converges along the rise of van der Waals interaction. Comparing Figs. 5(a) and (b) it is concluded that the rate of convergence of deflections for SS boundary conditions is more than CC, because the plate is more flexible in SS boundary

conditions, so the effect of the van der Waals interaction in governing equations would be more significant on decreasing and increasing the both deflections of upper and bottom layers.

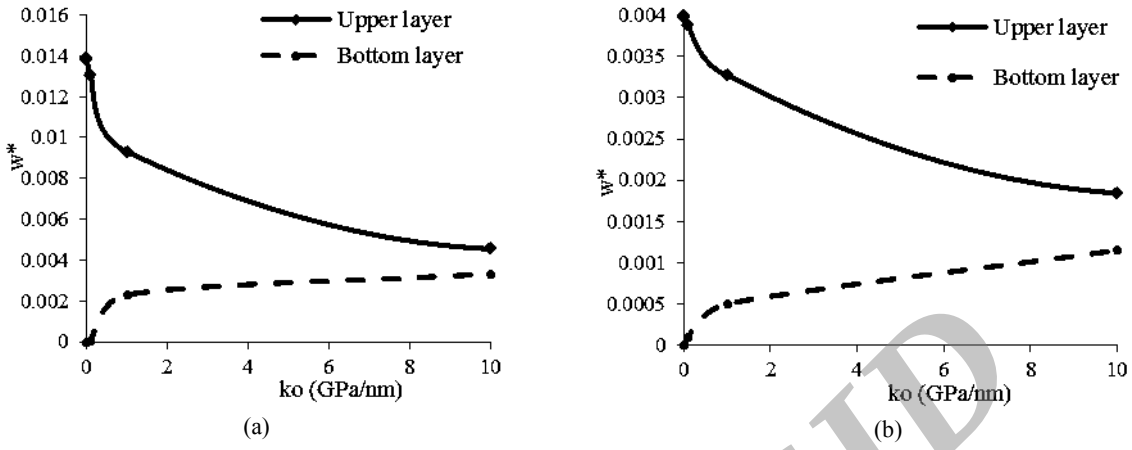

Fig.5
Variation of dimensionless deflection versus the van der Waals interaction between two layers (a) SS (b) CC boundary conditions

The various types of boundary conditions are assumed at two edges $r = r_i, r_o$. The maximum deflection of the upper layer due to nonlocal parameter variations is shown in Fig. 6. According to Fig. 6., The dimensionless deflection reduces with increase of nonlocal parameter. This concept shows that the flexibility of the nano plate decreases along the growing of nonlocal parameter. Furthermore, because of the more flexible boundary conditions and consequently the more effects of nonlocal parameter on the results, the curve slope for FC and FS boundary conditions are more than CC and SS.

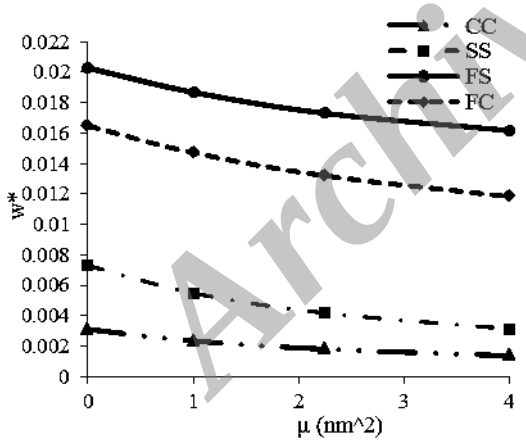

Fig.6
Variation of dimensionless deflection versus the nonlocal parameter for different types of boundary conditions.

Fig. 7. illustrates the deflection ratio between the linear and nonlinear FSDT analysis [28], along the increase of nonlocal parameter for both simply supported and clamped boundary conditions.

$$R_s = \frac{w_{Linear}}{w_{Nonlinear}} \tag{44}$$

As much as it was predictable, according to Fig. 7. the deflection in nonlinear FSDT is less than the linear analysis thru considering nonlinear strain terms and neglecting the effects of the rigidity deformations on the results. It is concluded that with increase of nonlocal parameter the linear and nonlinear analysis tends to each other. Also, it is observed that the curve slope for simply supported boundary conditions is more than clamped.

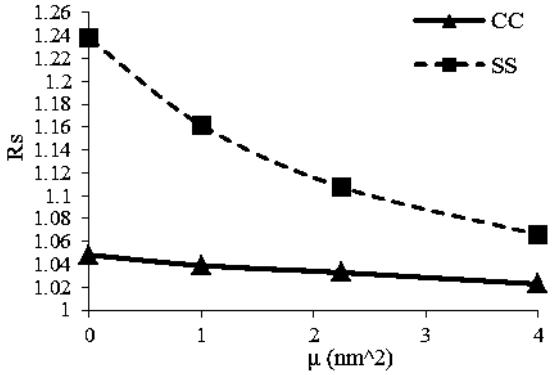

Fig.7
Variation of R_s versus the nonlocal parameter for C-C and S-S boundary condition.

The variation of R_m versus the dimensionless transverse loading is shown in Fig. 8. R_m is defined as [28]:

$$R_m = \frac{w_{Nonlocal}}{w_{local}} \tag{45}$$

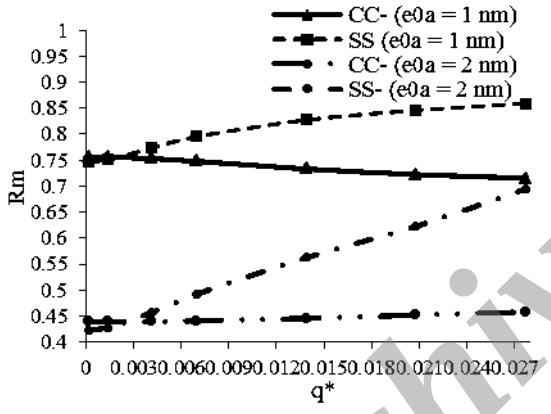

Fig.8
Variation of R_m versus the dimensionless transverse loading.

R_m shows the nonlocal effects on the results. In Fig. 8 the variation of R_m parameter is investigated based on various uniform transverse loads for both simply supported and clamped boundary conditions. As it is observed, with growing of transverse load, the nonlocal theory recedes from the local theory for clamped boundary conditions (CC). Also, these variations are inappreciable for greater nonlocal parameters. However, the both local and nonlocal theories approach along the rise of loads for simply supported boundary condition (SS). Also, with increase of nonlocal parameter, the variation of R_m is increased.

Sample 2: Bilayer circular plate

A bilayer circular nano plate is considered with the identities as follows (Fig. 9):

$$E_r = E_\theta = 1.06\times10^{12}\,\text{Pa};\ q^* = 4.5\times10^7 / E; k_w^* = 0.0018868;\ R^* = r_o/h = 7.35$$

The boundary conditions are as below:

At the center: $u^* = \psi^* = Q_r = 0$, Simply Supported : $u^* = w^* = M_r^* = 0$, Clamped : $u^* = w^* = \psi^* = 0$

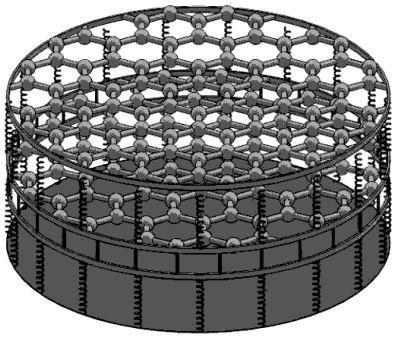

Fig.9
Bilayer Circular nano plate.

The variation of R_m for upper and bottom layers is shown in Fig. 10 in presence (a) and absence of elastic foundation (b) versus the van der Waals interaction between the layers for clamped circle.

As shown, increase of van der Waals interaction value causes decreasing the R_m parameter. The local and nonlocal analysis recedes from each other long the rise of k_o for upper layer in presence and absence of elastic foundation. However, the local and nonlocal results approach versus the increase of k_o in absence of elastic foundation (Fig. 10 (a)). When the elastic foundation exists, increasing the van der Waals interaction causes approaching the local and nonlocal results up to a specific value of k_o. In continue, with increase of k_o, the local and nonlocal results are receded. Also, it can be seen that the variation of R_m is more significant when the small scale effects are increased.

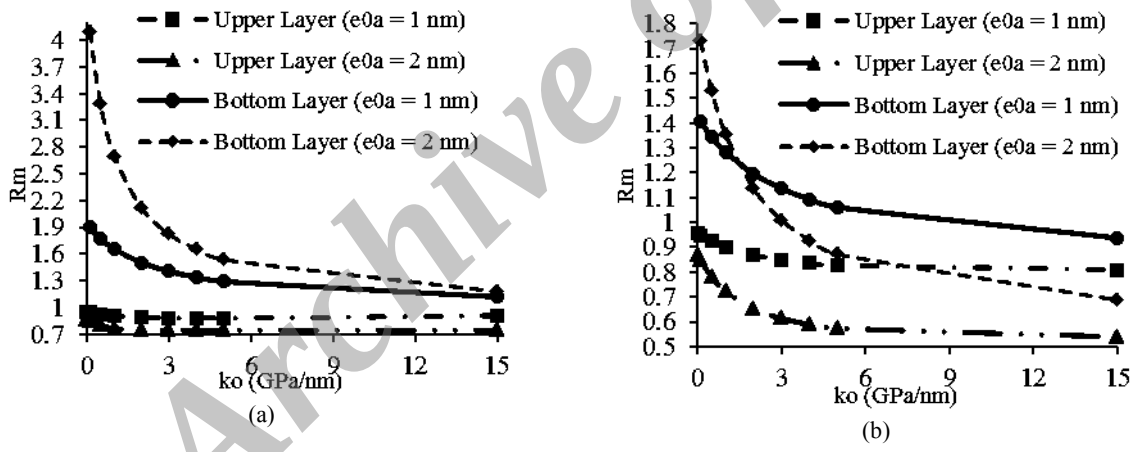

Fig.10
Variation of R_m versus the van der Waals interactions value for upper and bottom layers in absence (a), presence of elastic foundation (b).

Finally, the effect of Winkler-Pasternak elastic foundation is studied for two types of boundary conditions clamped and simply supported edges in Fig. 11. The effect of Winkler elastic foundation is studied in Fig. 11(a). As shown, with increase of Winkler stiffness value up to 1 GPa/nm, the maximum deflection descends with a steep slope, then it tends to a constant value. In continue, there are not any considerable changes in deflection descending. It is observed that the deflections are receded with increase of the non-local parameter along the growing of Winkler elastic foundation up to a specific value near 1 GPa/nm. In continue, the deflections approach with rise of the Winkler stiffness and the effect of small scales decreases. The variation is extremely considerable for simply supported boundaries in comparison with clamped. It is observed that the results for two types of boundary conditions tend to each other with a gradual slope with increasing the Winkler stiffness more than 1 GPa/nm. Accordingly, it is concluded that the value of Winkler stiffness matrix has more effects on the decreasing of the deflection. As shown in Fig. 11(b), all the mentioned results for Winkler elastic foundation is correct for the

Pasternak. However, the descending procedure for deflection along the increase of Pasternak stiffness continues gently and the maximum deflections are not so close for two types of boundary conditions, as they are for the Winkler stiffness matrix.

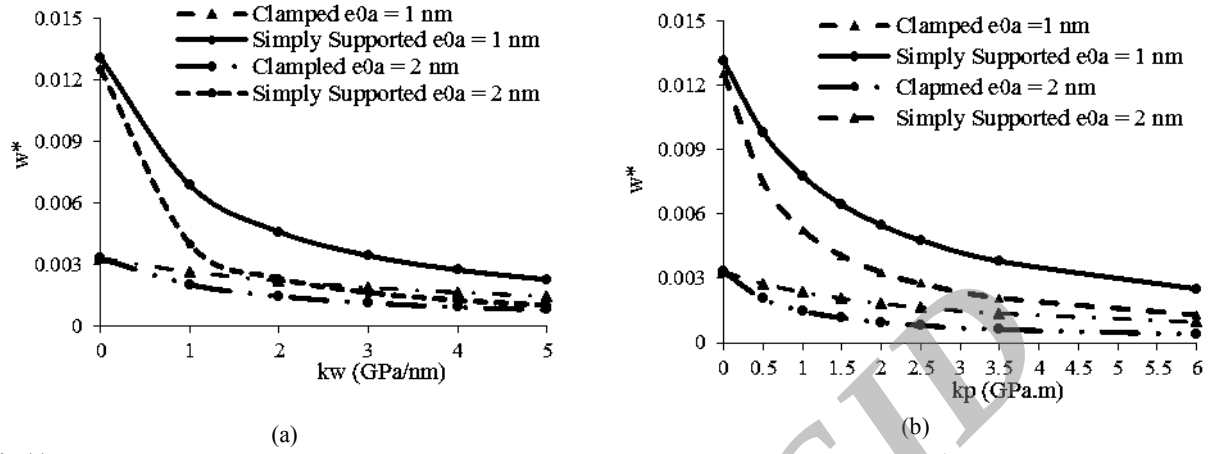

Fig.11
Dimensionless deflection versus (a) Winkler stiffness foundation. (b) Pasternak stiffness foundation.

6 CONCLUSIONS

In this paper, the nonlinear bending analysis of bilayer annular/circular graphene sheets embedded in two parameters Winkler-Pasternak elastic matrix was investigated based on the nonlocal elasticity theory. The equilibrium equations were derived using the principals of minimum potential energy method. The driven ordinary differential equations were solved using the differential quadrature method (DQM) which is a highly accurate numerical method and a new semi-analytical polynomial method (SAPM). The effects of nonlocal parameter, van der Waals interaction between the layers, elastic foundation, transverse load and the boundary conditions were studied. The total conclusions can be categorized as follows:

- The presented semi-analytical polynomial method (SAPM) is highly accurate, considerably simple in formulations and programming. Its rate of processing time is about fifty percent more than DQM. So, it can be used instead of the other popular numerical methods.
- The deflection of the upper and bottom layers approach to each other with increase of the van der Waals interaction.
- Increase of nonlocal parameter leads to decreasing the deflections for upper layer in all types of boundary conditions. Whatever the plate is more flexible in boundary conditions, the small scale effects on the results increases.
- Increasing the nonlocal parameter has much more effects on nonlinear analysis in comparison with the linear analysis.
- The effects of growing the nonlocal parameter on deflection increases when the plate is embedded in an elastic foundation.
- If elastic foundation exists, the local and nonlocal theories will recede along the rise of loading. On contrary, two theories approach in absence of elastic foundation.
- The Winkler stiffness value has the more effects on the deflection's descending in comparison with the Pasternak elastic foundation.

REFERENCES

[1] Androulidakisa Ch., Tsouklerib G., Koutroumanisa N., Gkikasb G., Pappasb P., Partheniosb K., Papagelisa J., Galiotisb C., 2015, Experimentally derived axial stress–strain relations for two-dimensional materials such as monolayer graphene, *Carbon* **81**:322-328.

[2] Reddy J.N., 2011, Microstructure-dependent couple stress theories of functionally graded beams, *Journal of the Mechanics and Physics of Solids* **59**: 2382-2399.
[3] Akgöz B., Civalek Ö., 2013, A size-dependent shear deformation beam model based on the strain gradient elasticity theory, *International Journal of Engineering Science* **70**: 1-14.
[4] Akgöz B., Civalek Ö., 2013, Buckling analysis of functionally graded micro beams based on the strain gradient theory, *Acta Mechanica* **224**: 2185-2201.
[5] Lam D.C.C., Yang F., Chong A.C.M., Wang J., Tong P., 2003, Experiments and theory in strain gradient elasticity, *Journal of the Mechanics and Physics of Solids* **51**: 1477-1508.
[6] Ke L.L., Yang J., Kitipornchai S., 2012, Free vibration of size dependent Mindlin micro plates based on the modified couple stress theory, *Journal of Sound and Vibration* **331**: 94-106.
[7] Akgöz B., Civalek Ö., 2011, Strain gradient elasticity and modified couple stress models for buckling analysis of axially loaded micro scaled beams, *International Journal of Engineering Science* **49**: 1268-1280.
[8] Akgöz B., Civalek Ö., 2013, Free vibration analysis of axially functionally graded tapered Bernoulli-Euler microbeams based on the modified couple stress theory, *Composite Structures* **98**: 314-322.
[9] Yang F., Chong A.C.M., Lam D.C.C., Tong P., 2002, Couple stress based strain gradient theory for elasticity, *International Journal of Solids and Structures* **39**: 2731-2743.
[10] Eringen A.C., Edelen D.G.B., 1972, On nonlocal elasticity, *International Journal of Engineering Science* **10**: 233-248.
[11] Eringen A.C., 1983, On differential equations of nonlocal elasticity, solutions of screw dislocation, surface waves, *Journal of Applied Physics* **54**: 4703-4710.
[12] Eringen A.C., 2002, *Nonlocal Continuum Field Theories*, Springer-Verlag, New York.
[13] Eringen A.C., 2006, Nonlocal continuum mechanics based on distributions, *International Journal of Engineering Science* **44**: 141-147.
[14] Anjomshoa A., Shahidi A.R., Shahidi S.H., Nahvi H., 2014, Frequency analysis of embedded orthotropic circular and elliptical micro/nano-plates using nonlocal variational principle, *Journal of Solid Mechanics* **7**(1): 13-27.
[15] Kitipornchai S., He X.Q., He, K.M., Liew, 2005, Continuum model for the vibration of multilayered graphene sheets. *Physical Review B* **72**: 075443.
[16] He X.Q., Kitipornchai S., Liew K.M., 2005, Buckling analysis of multi-walled carbon nanotubes: a continuum model accounting for van der Waals interaction, *Journal of the Mechanics and Physics of Solids* **53**: 303-326.
[17] Liew K.M., He X.Q., Kitipornchai S., 2006, Predicting nanovibration of multi-layered graphene sheets embedded in an elastic matrix, *Acta Materialla* **54**: 4229-4236.
[18] Ghorbanpour Arani A., Kolahchi R., Allahyari S.M.R., 2014, Nonlocal DQM for large amplitude vibration of annular boron nitride sheets on nonlinear elastic medium, *Journal of Solid Mechanics* **6**(4): 334-346.
[19] Scarpa F., Adhikari S., Gil A.J., Remillat C., 2010, The bending of single layer graphene sheets: The lattice versus continuum approach, *Nanotechnology* **21**: 125702.
[20] Murmu T., Pradhan S.C., 2009, Thermo-mechanical vibration of a single-walled carbon nanotube embedded in an elastic medium based on nonlocal elasticity theory, *Computational Material Science* **46**: 854-859.
[21] Ke L.L., Xiang Y., Yang J., Kitipornchai S., 2009, Nonlinear free vibration of embedded double-walled carbon nanotubes based on nonlocal Timoshenko beam theory, *Computational Material Science* **47**: 409-417.
[22] Dong Y.X., LIM C.W., 2009, Nonlinear vibrations of nano-beams accounting for nonlocal effect using a multiple scale method, *Science in China Series E, Technological Sciences* **52**: 617-621.
[23] Ansari R., Rajabiehfard R., Arash B., 2010, Nonlocal finite element model for vibrations of embedded multi-layered graphene sheets, *Computational Material Science* **49**: 831-838.
[24] Pradhan S.C., Phadikar J.K., 2009, Small scale effect on vibration of embedded multilayered graphene sheets based on nonlocal continuum models, *Physica Letter A* **373**: 1062-1069.
[25] Pradhan S.C., Kumar A., 2010, Vibration analysis of orthotropic graphene sheets embedded in Pasternak elastic medium using nonlocal elasticity theory and differential quadrature method, *Computational Material Science* **50**: 239-245.
[26] Yang J., Ke L.L., Kitipornchai S., 2010, Nonlinear free vibration of single-walled carbon nanotubes using nonlocal Timoshenko beam theory, *Physica E* **42**: 1727-1735.
[27] Shen L., Shen H.S., Zhang C.L., 2010, Nonlocal plate model for nonlinear vibration of single layer graphene sheets in thermal environments, *Computational Material Science* **48**: 680-685.
[28] Golmakani M.E., Rezatalab J., 2014, Nonlinear bending analysis of orthotropic nanoscale plates in an elastic matrix based on nonlocal continuum mechanics, *Composite Structures* **111**: 85-97.
[29] Mohammadi M., Goodarzi M., Ghayour M., AlivandS., 2012, Small scale effect on the vibration of orthotropic plates embedded in an elastic medium and under biaxial in-plane pre-load via nonlocal elasticity theory, *Journal of Solid Mechanics* **4**(2): 128-143.
[30] Bellman R.E., Casti J., 1971, Differential quadrature and long-term integration, *Journal of Mathematical Analysis & Applications* **34**: 235-238.
[31] Bellman R.E., Kashef B.G., Casti J., 1972, Differential Quadrature: A Technique for the Rapid Solution of Nonlinear Partial Differential Equation, *Journal of Computational Physics* **10**: 40-52.
[32] Altekin M., Yükseler R.F., 2011, Large deflection analysis of clamped circular plates, *Proceedings of the World Congress on Engineering*, London, UK.

[33] Timoshenko S., Woinowsky-Krieger S., 1959, *Theories of Plates and Shells*, McGraw- Book Company, New York.
[34] Szilard R., 1974, *Theory and Analysis of Plates*, Englewood Cliffs, Prentice-Hall nc.
[35] Reddy J.N., Wang C.M., Kitipornchai S., 1999, Axisymmetric bending of functionally grade circular and annular plates, *European Journal of Mechanical A/Solids* **18**: 185-199.
[36] Golmakani M.E., 2014, Nonlinear bending analysis of ring-stiffened functionally graded circular plates under mechanical and thermal loadings, *International Journal of Mechanical Science* **79**: 130-142.